

## **Blade Design Trade-Offs Using Low-Lift Airfoils for Stall-Regulated HAWTs**

P. Giguère and M.S. Selig  
University of Illinois at Urbana-Champaign

J.L. Tangler  
National Renewable Energy Laboratory

*Presented at the ASME/AIAA Wind  
Energy Symposium  
Reno, Nevada  
January 11-14, 1999*



**NREL**

National Renewable Energy Laboratory

1617 Cole Boulevard  
Golden, Colorado 80401-3393

NREL is a U.S. Department of Energy Laboratory  
Operated by Midwest Research Institute • Battelle • Bechtel

Contract No. DE-AC36-98-GO10337

## NOTICE

This report was prepared as an account of work sponsored by an agency of the United States government. Neither the United States government nor any agency thereof, nor any of their employees, makes any warranty, express or implied, or assumes any legal liability or responsibility for the accuracy, completeness, or usefulness of any information, apparatus, product, or process disclosed, or represents that its use would not infringe privately owned rights. Reference herein to any specific commercial product, process, or service by trade name, trademark, manufacturer, or otherwise does not necessarily constitute or imply its endorsement, recommendation, or favoring by the United States government or any agency thereof. The views and opinions of authors expressed herein do not necessarily state or reflect those of the United States government or any agency thereof.

Available to DOE and DOE contractors from:  
Office of Scientific and Technical Information (OSTI)  
P.O. Box 62  
Oak Ridge, TN 37831  
Prices available by calling 423-576-8401

Available to the public from:  
National Technical Information Service (NTIS)  
U.S. Department of Commerce  
5285 Port Royal Road  
Springfield, VA 22161  
703-605-6000 or 800-553-6847  
or  
DOE Information Bridge  
<http://www.doe.gov/bridge/home.html>



# BLADE DESIGN TRADE-OFFS USING LOW-LIFT AIRFOILS FOR STALL-REGULATED HAWTS

Philippe Giguère\* and Michael S. Selig†  
University of Illinois at Urbana-Champaign  
Urbana, IL 61801

James L. Tangler‡  
National Renewable Energy Laboratory  
Golden, CO 80401

## Abstract

A systematic blade design study was conducted to explore the trade-offs in using low-lift airfoils for a 750-kilowatt stall-regulated wind turbine. Tip-region airfoils having a maximum lift coefficient ranging from 0.7–1.2 were considered in this study, with the main objective of identifying the practical lower limit for the maximum lift coefficient. Blades were optimized for both maximum annual energy production and minimum cost of energy using a method that takes into account aerodynamic and structural considerations. The results indicate that reducing the maximum lift coefficient below the upper limit considered in this study increases the cost of energy independently of the wind regime. As a consequence, higher maximum lift coefficient airfoils for the tip-region of the blade become more desirable as machine size increases, as long as they provide gentle stall characteristics. The conclusions are applicable to large wind turbines that use passive or active stall to regulate peak power.

## 1. Introduction

The use of aerodynamic stall is a common means of regulating peak power for horizontal axis wind turbines (HAWTs) operating at constant speed. Stall regulation can be performed either actively (pitch control) or passively (fixed pitch), the latter being the more popular approach. For both of these approaches, the stall characteristics of the airfoils used over the tip region of the blades are important because they strongly affect the dynamics of the rotor, and thus the structural design of the blades. Reducing blade dynamic excitations, such as stall-induced vibrations, can be achieved using airfoils having a gentle stall, which typically have a low maximum lift coefficient ( $c_{l,max}$ ), i.e., low-lift airfoils. In contrast, high-lift airfoils often have an abrupt or hard stall that is characterized by a rather large loss in lift and negative lift-curve slope. As a result, high-lift airfoils increase blade dynamic excitations as compared with low-lift airfoils. The use of high-lift airfoils, however, is beneficial for minimizing blade solidity and enhancing starting torque. Also, for a given amount of laminar flow, high-lift airfoils are more efficient (higher lift-to-drag ratio) than airfoils with a low  $c_{l,max}$ . Therefore, there are design trade-offs in selecting the lift range of the airfoils for a particular rotor.

The trade-offs between low-lift and high-lift airfoils for stall-regulated HAWTs have been recognized for some time now. Since 1984, the National Renewable Energy Laboratory (NREL), in collaboration with Airfoils Inc., have developed over 10 airfoil families specifically for wind turbines. Most tip-region airfoils have a low  $c_{l,max}$ , in the range of 0.9–1.2, while the root airfoils have a higher  $c_{l,max}$ .<sup>1–3</sup> Another important characteristic of the NREL airfoils is that their  $c_{l,max}$  is less sensitive to roughness effects as

---

\* Graduate Research Assistant, Aeronautical and Astronautical Engineering Department.

† Associate Professor, Aeronautical and Astronautical Engineering Department.

‡ Senior Scientist, National Wind Technology Center.

*The results of this paper were presented at the ASME Wind Energy Symposium, Reno, NV, January 11-14, 1999.*

compared with airfoils that were designed for aircraft applications and used on wind turbines.<sup>3</sup> Blades for both experimental and commercial wind turbines have successfully used the NREL airfoils.<sup>4-6</sup> The approach of using a high-lift airfoil for the inboard part of the blade and low-lift airfoils for the tip region has also been reiterated in a recent report from Risø.<sup>7</sup> More precisely, this report states that high-lift airfoils are desirable inboard to obtain a slender blade and low lift-airfoils should be preferred outboard to minimize negative aerodynamic damping.

Even though the importance of using low-lift airfoils in the tip region has been recognized,<sup>3,7</sup> it is unclear if there is merit in considering airfoils having a lower  $c_{l,max}$  than that of the NREL airfoils. Accordingly, the present research effort focused on identifying the practical lower limit of the maximum lift coefficient within the range of 0.7–1.2 for airfoils tailored for stall-regulated wind turbines. Another objective was to investigate the effects of increasing swept area by reducing  $c_{l,max}$  in the blade-tip region. To carry out those two objectives, a method for rotor optimization that takes into account both aerodynamic and structural considerations was developed. The blade design method, which is described in Section 2, was used to perform a systematic blade design trade-off study for a 750-kilowatt (kW) stall-regulated HAWT. The results of this study are presented and discussed in Section 3. Section 4 provides the conclusions, which are applicable to large wind turbines that use passive or active stall to regulate peak power.

## 2. Blade Design Method

The blade design approach section is subdivided into six subsections, namely: (1) design approach, (2) design constraints, (3) annual energy production computation, (4) cost of energy computation, (5) airfoil data, (6) case matrix and optimization cases.

### 2.1 Design approach

The blade design trade-off study was performed using the computer program PROPGA,<sup>8,9</sup> which is a genetic algorithm based optimization method for the blade geometry of HAWTs. In brief, PROPGA mimics Darwin's theory of the survival of the fittest over a population of candidate blade shapes that evolves from one generation to the next. Blade designs having a large fitness according to the objective function for the optimization process have a larger probability to “reproduce” in creating the new generations compared with those with a small fitness value. A binary string represents each candidate blade geometry, and the reproduction process involves crossover and mutation operators. More details about PROPGA can be found in Refs. 8 and 9.

In this work, two objective functions were considered: maximum annual energy production (AEP) and minimum cost of energy (COE). For the optimization for maximum AEP, PROPGA was used to determine the optimum chord and twist distributions as well as the blade pitch for a given airfoil family. The chord and twist/pitch were optimized at four radial stations (15%, 40%, 75%, and 95% radius) and a cubic spline was used to obtain the chord and twist values at each blade segment. In optimizing for minimum COE, PROPGA provided the optimum rotor diameter in addition to the optimum chord, twist, and pitch. The computer program PROPID,<sup>9,10</sup> which is an inverse design method for HAWTs based on the PROP code,<sup>11-12</sup> was used to analyze the rotor performance of the candidate blade designs. The AEP was computed by PROPID while the COE computations were performed by PROPGA.

The following PROPGA and PROPID settings were used:

- Population size of 252
- String length of 56 bits for AEP optimization and 63 bits for COE optimization (7 bits per parameter)
- A total of 25 generations
- Tournament selection
- Uniform crossover with a 50% probability

- Mutation rate of 1%
- Elitism on (best blade design of one generation is copied as is into the subsequent generation)
- Niching on all parameters<sup>9</sup>
- 10 blade segments
- Prandtl tip-loss model
- Swirl on
- Corrigan post-stall model<sup>13</sup>
- Sea-level atmospheric conditions

## 2.2 Design constraints

The trade-off study was conducted for a three-blade, upwind, fixed-pitch, 750-kW HAWT having a baseline rotor diameter of 44 m. In the optimization process, the inverse design capability of PROPID was used to ensure a rated power of 750 kW by iterating on blade pitch. For noise considerations, the tip speed was fixed at 62 m/s, which corresponds to 27 revolutions per minute (rpm) for the baseline rotor diameter. Therefore, the rpm was adjusted according to the rotor diameter for the case of the optimization for minimum COE. Airfoil families made up of three airfoils (root, primary, and tip airfoils) were considered. The distribution of these airfoils along the blade and their respective thickness was fixed, i.e., root airfoil (24% thick) up to 40% radius, primary airfoil (21% thick) at 75% radius, and tip airfoil (16% thick) at 95% radius. This airfoil distribution is that of the NREL thick-airfoil families.<sup>3</sup>

## 2.3 Annual energy production computation

PROPID generated a power curve from the cut-in to cut-out wind speed of 25 m/s, with a 1 m/s increment. The power curves reflected the enhanced lift inboard of the blade owing to stall delay as modeled with the Corrigan post-stall model.<sup>13</sup> A Rayleigh wind speed distribution was used in computing the AEP. Two wind classes of the International Electrotechnical Commission (IEC) were considered, namely class II and IV having an average wind speed of 8.5 m/s and 6 m/s, respectively. No losses were considered, and thus the AEP values presented in this paper represent the gross output.

## 2.4 Cost of energy computation

The COE was calculated using the following expression:

$$COE = \frac{(TC + BOS)}{AEP} FCR + O \& M \quad (1)$$

In this equation, the turbine cost  $TC$  was based on blade cost assuming that the blades represent 20% of the total turbine cost. The blade cost was determined according to a weight estimate for E-glass using a price of \$20/kg, which includes labor, overhead, and profit. For the balance of station  $BOS$  a cost of \$200/kW was considered, thus fixing the  $BOS$  to \$150,000 for a 750-kW turbine. The fixed charge rate  $FCR$  was 11% and a 98% availability was applied to the annual energy production  $AEP$ . Finally, a fixed cost of \$0.01/kWh was used for operation and maintenance  $O \& M$ . The value of 20% for the blade cost over total turbine cost and the  $BOS$ ,  $FCR$ , and  $O \& M$  costs were obtained from discussions with NREL personnel. This COE model is simplistic, but the results will show that this was an appropriate model for this study.

In estimating the blade weight, the hub (5% of blade span) was modeled as a tube, and the airfoil section was modeled as an I-beam without a shear web, as shown in Fig. 1. This modeling approach has been used in other wind turbine optimization work.<sup>14</sup> The hub skin thickness is  $t_{sH}$  and the chord or diameter of

the hub is  $c_H$ . For the airfoil section at a given blade segment,  $t_{sA}$  is the skin thickness,  $c$  is the chord, and  $t$  is the physical thickness. It is important to note that in this modeling of the airfoil section, the skin as shown in Fig. 1b is not the actual spar but rather a representation of the overall skin thickness that is carrying the load.

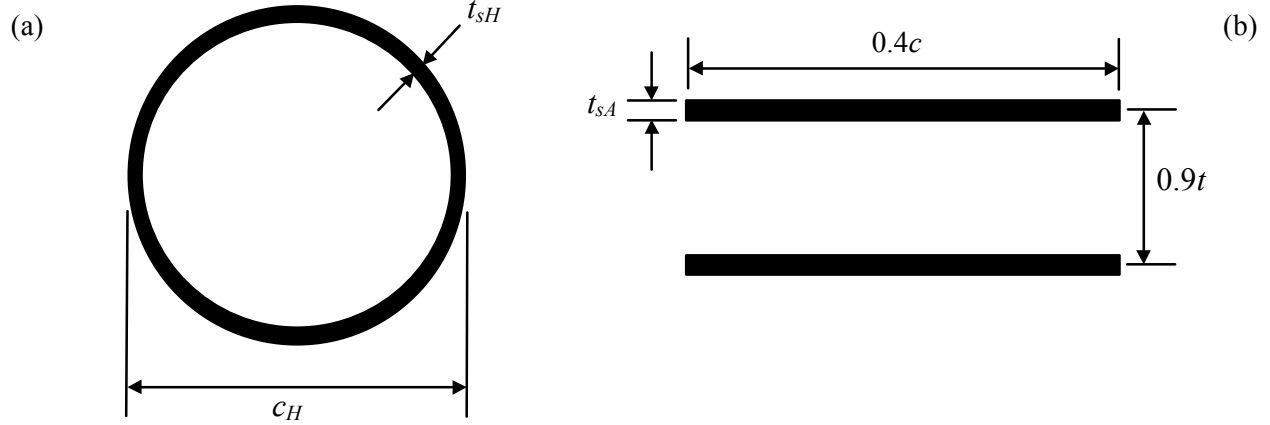


Fig. 1: Modeling of the (a) hub and (b) the airfoil section for estimating the blade weight.

The procedure for estimating the blade weight began with the computation of the flap-bending loads at each blade segment from the thrust distribution for a given load condition. Even though there are many design load cases in the IEC standards,<sup>15</sup> the ultimate flap-bending loads were taken as the critical case to consider because of the inverse relationship between the  $c_{l,max}$  of the airfoils used and the resulting blade area. As mentioned in the introduction, the use of high-lift airfoils will minimize the blade solidity for a given swept area as compared with the use of low-lift airfoils. Accordingly, the IEC 50-year extreme wind speed<sup>15</sup> for either a wind class II (59.5 m/s) or IV (42 m/s) was used in this study to compute the blade loads when the rotor is parked and fully exposed to the wind (worst-case hurricane condition). The IEC load factor of 1.35 was applied to the static flap-bending loads. Using the static flap-bending load  $M$  for a given blade segment or radial position  $r$ , the required moment of inertia  $I$  for that segment to match a prescribed stress level  $s_p$  along the blade was computed according to Eq. 2. The skin thickness  $t$  in Eq. 2 represents either that of the hub or the airfoil section for a given blade segment.

$$I(r) = \frac{M(r)[t(r)/2]}{s_p(r)} \quad (2)$$

The prescribed stress level for each blade segment was derived from an allowable stress for E-glass, which was the material of choice for this study, using a safety margin that decreased linearly from 2.0 at the root to 1.5 at the tip. Under an ultimate strength test, failure of E-glass blades typically occurs at approximately 4000 micro strains,<sup>16</sup> which corresponds to a material strength of 110 MPa. To account for residual stresses, an allowable stress level of 94 MPa was used (15% knockdown).

Given the required moment of inertia at each blade segment, the required skin thickness was then determined from Eqs. 3 and 4 for the hub and airfoil sections, respectively.

$$t_{sH} = \frac{I_H}{\pi \left( \frac{c_H^3}{8} \right)^{\frac{1}{3}}} \quad (3)$$

$$t_{sA}(r) = \frac{I(r)}{(81/500)ct^2} \quad (4)$$

Note that the contribution of the skin about its own rotational axis was neglected in the expression of the moment of inertia of the airfoil section because it is much smaller than the inertia resulting from the distance of the material from the neutral axis. Also, the minimum skin thickness was set to 5 mm.

From the skin thickness distribution along the blade obtained from Eqs. 3 and 4, the blade cross-sectional area at each segment was calculated according to Fig. 1. Practically, however, not all the skin of the blade is carrying the load. Consequently, the minimum skin thickness was applied to the airfoil perimeter along the leading and trailing edges. The blade material volume was then computed from linear extrapolations of the local cross-sectional area of each of the 10 blade segments. Finally, the blade weight was obtained using a density of 2000 kg/m<sup>3</sup>, which is representative of E-glass. Figure 2 summarizes the process of computing COE.

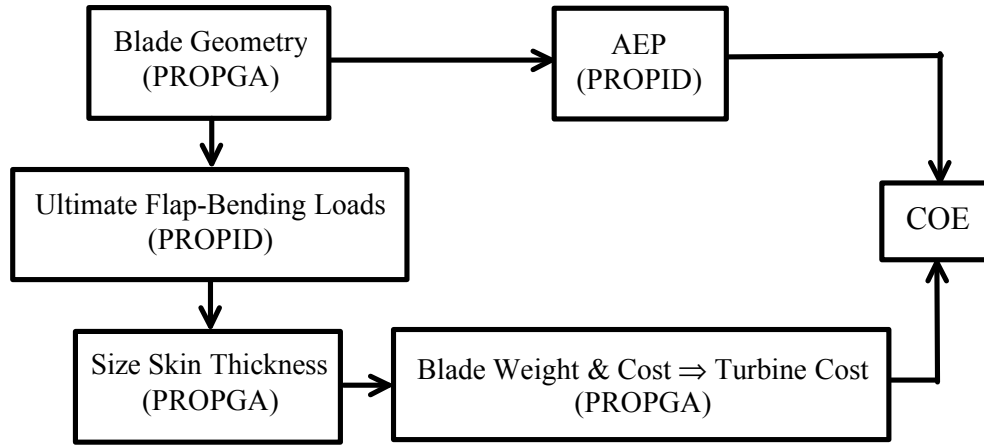


Fig. 2: Flow chart outlining the different steps to compute COE.

## 2.5 Airfoil data

Because of the limited amount of aerodynamic data on low  $c_{l,max}$  airfoils designed for large HAWTs and short of designing airfoils specifically for this work, synthesized airfoil data covering a  $c_{l,max}$  range of 0.7–1.2 was generated for this study. This synthesized airfoil data was based on Eppler code<sup>17</sup> predictions for the NREL S818 (root,  $c_{l,max}$  of 1.4), S827 (primary,  $c_{l,max}$  of 1.0), and S828 (tip,  $c_{l,max}$  of 0.9) airfoils, which form one of the NREL thick-airfoil families for extra-large blades (referred to here as the baseline airfoil family).<sup>3</sup> Data was synthesized for a total of five airfoil families including the baseline family. The S818 was used as the common root airfoil for all families. The primary and tip airfoils had  $c_{l,max}$  between 0.8–1.2 and 0.7–1.1, respectively. Figure 3 presents the synthesized data for the five primary airfoils.

The method used to obtain the synthesized data from the lift and drag coefficients ( $c_l$  and  $c_d$ ) of the S827 and S828 was to add a  $c_l$  increment ( $\Delta c_l$ ) to attain the desired  $c_{l,max}$  and modify the  $c_d$  values using a scale factor, which depended on the  $\Delta c_l$ . More precisely, the  $c_d$  scale factor was set to 1.0 for negative  $\Delta c_l$  while values of 1.0375 and 1.075 were used for  $\Delta c_l$  of 0.1 and 0.2, respectively. These  $c_d$  scale factors were derived from Eppler predictions for other NREL airfoils, namely the S816, S817, and S829, which were also designed for extra-large blades.<sup>3</sup> Because of the shortcomings of the Eppler code and other

computational airfoil analysis programs in accurately predicting  $c_{l,max}$  and data beyond stall, results from the Delft wind tunnel tests for the S809<sup>18</sup> and S814<sup>19</sup> airfoils were used to extend the data into stall. Therefore, the root S818 airfoil had a harder stall than that for the primary and tip airfoils, which used the S809 stall characteristics. The roughness effects were not modeled in this study because a recent report indicated that roughness effects on aft-cambered NREL airfoils are mainly driven by airfoil thickness and not  $c_{l,max}$ .<sup>20</sup> In this study, the airfoil thickness distribution is the same for all airfoil families. Therefore, roughness losses can be considered to be essentially the same owing to the similarity in the airfoils' characteristics.

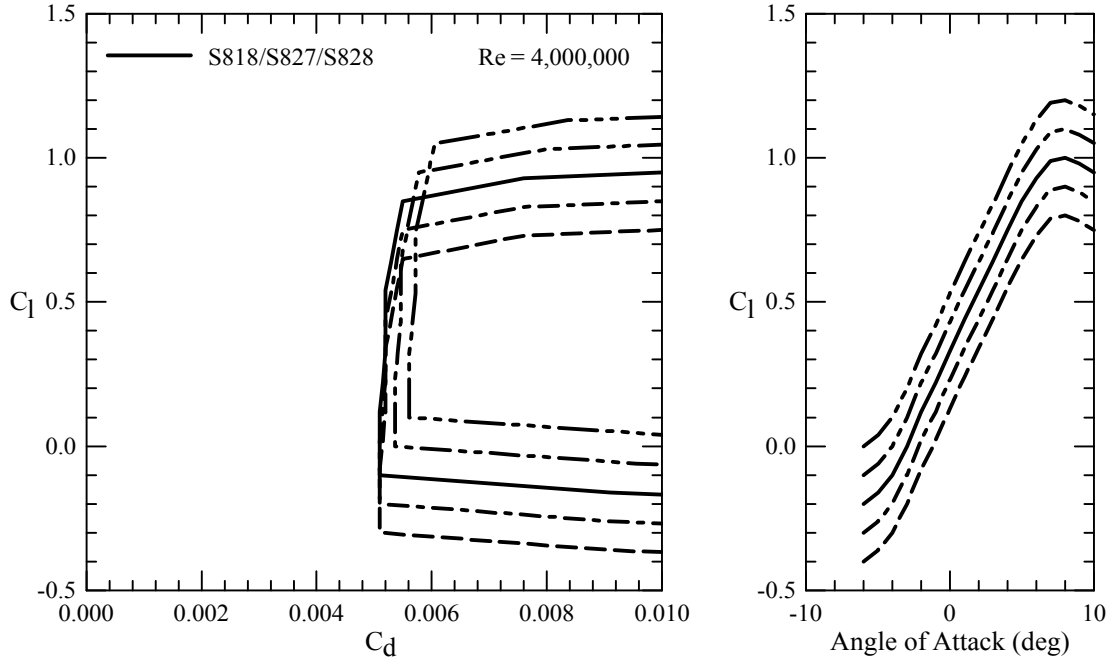


Fig. 3: Synthesized airfoil data for the primary airfoils based on the NREL S827 airfoil.

Although not presented in this paper, the airfoil data covered the Reynolds number range of  $2\text{--}5 \times 10^6$  with an increment of  $1 \times 10^6$ . Furthermore, the Corrigan post-stall model<sup>13</sup> was used to modify the two-dimensional data for three-dimensional and rotational effects. In terms of using the data, linear interpolation was used between airfoil data files for stations where there is a blend of airfoils. The use of these airfoil data files allows for the interpolation/extrapolation of the data with Reynolds numbers. Linear interpolation is used for lift, and logarithmic interpolation is used for drag to accurately represent the airfoil characteristics. Note that extrapolation of the data is not performed for Reynolds numbers smaller than the minimum Reynolds number in each airfoil data file, i.e.,  $2 \times 10^6$ .

## 2.6 Case matrix and optimization cases

The case matrix used for this study is shown in Table 1. A total of five design cases were considered representing the five airfoil families. The airfoil names starting with “75” represent the primary airfoils that are located at 75% radius while those beginning with “95” (95% radius) are the tip airfoils. Again, the root airfoil was the same for all airfoil families, and thus it has been omitted in Table 1. Each airfoil name has a two-digit number by the “75” or the “95” representing the  $c_{l,max}$  of that airfoil. Therefore, airfoil 75-08 is a primary airfoil with a  $c_{l,max}$  of 0.8. All cases or airfoil families have a  $c_{l,max}$  that decreases from root to tip, in a similar fashion to the NREL airfoil families. Case 10-09 represents the baseline airfoil family.



Table 1: Case matrix.

Airfoils	95-07	95-08	95-09	95-10	95-11
75-08	c08-07	–	–	–	–
75-09	–	c09-08	–	–	–
75-10	–	–	c10-09	–	–
75-11	–	–	–	c11-10	–
75-12	–	–	–	–	c12-11

As mentioned in subsection 2.1, optimizations were performed for both maximum AEP and minimum COE, which represent the two optimization cases. The optimizations for maximum AEP were performed for IEC wind class II under two scenarios. In the first scenario, the rotor diameter was fixed to the baseline value of 44 m. For the second scenario, the rotor diameter was increased with decreasing  $c_{l,max}$ . Table 2 indicates the increase in diameter and corresponding increase in swept area for each of the five cases. The optimization for minimum COE, for which the rotor diameter was a free variable, was carried out for IEC wind classes II and IV. Overall, a total of 20 PROPGA runs were performed in this study.

Table 2: Increase in rotor diameter and swept area for the five design cases.

Case	Diameter (m)	% Incr.	Swept Area (m <sup>2</sup> )	% Incr.
c08-07	23.10	5.0	1676.4	10.3
c09-08	22.88	4.0	1644.6	8.2
c10-09	22.66	3.0	1613.1	6.1
c11-10	22.44	2.0	1582.0	4.0
c12-11	22.22	1.0	1551.1	2.0

### 3. Results and Discussion

This section presents the results for AEP and COE for each of the five cases shown in the case matrix (see Table 1). In addition, the chord distribution for each case is depicted. The results for the two optimization cases are presented and discussed separately.

#### 3.1 Optimization for maximum AEP

Figure 4 shows the AEP for the five design cases. Clearly, the AEP is basically the same for all cases when the rotor diameter was fixed (maximum difference of 0.3%). As expected, the AEP scales with the increase in rotor diameter, with a maximum difference of 3% in AEP.

The blades that were optimized for maximum AEP were also analyzed for loads and cost to provide COE estimates, which are presented in Fig. 5. These COE results indicate an advantage in using the highest  $c_{l,max}$  case, particularly when the rotor diameter was fixed. Increasing rotor diameter with decreasing  $c_{l,max}$  helped reduce COE, but the higher  $c_{l,max}$  cases (cases 11-10 and 12-11) provided the lowest COE. The lower COE of the higher  $c_{l,max}$  cases can be explained by the chord distributions depicted in Fig. 6. For a given rated power, the blade area is inversely proportional to the  $c_{l,max}$  of the airfoils used. Therefore, the lower  $c_{l,max}$  cases resulted in broad outboard chord lengths, thereby resulting in higher blade loads under the 50-year extreme wind condition and larger overall cost of the turbine. The inboard chord distributions were mostly similar because the same root airfoil was used.

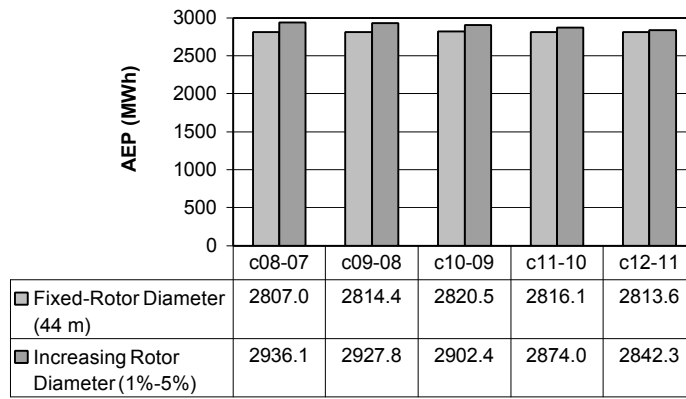


Fig. 4: Annual energy production for the cases considered in the optimization for maximum AEP.

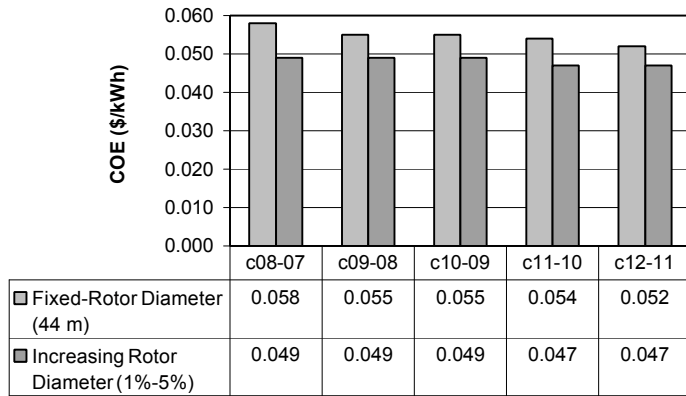


Fig. 5: Cost of energy for the cases considered in the optimization for maximum AEP.

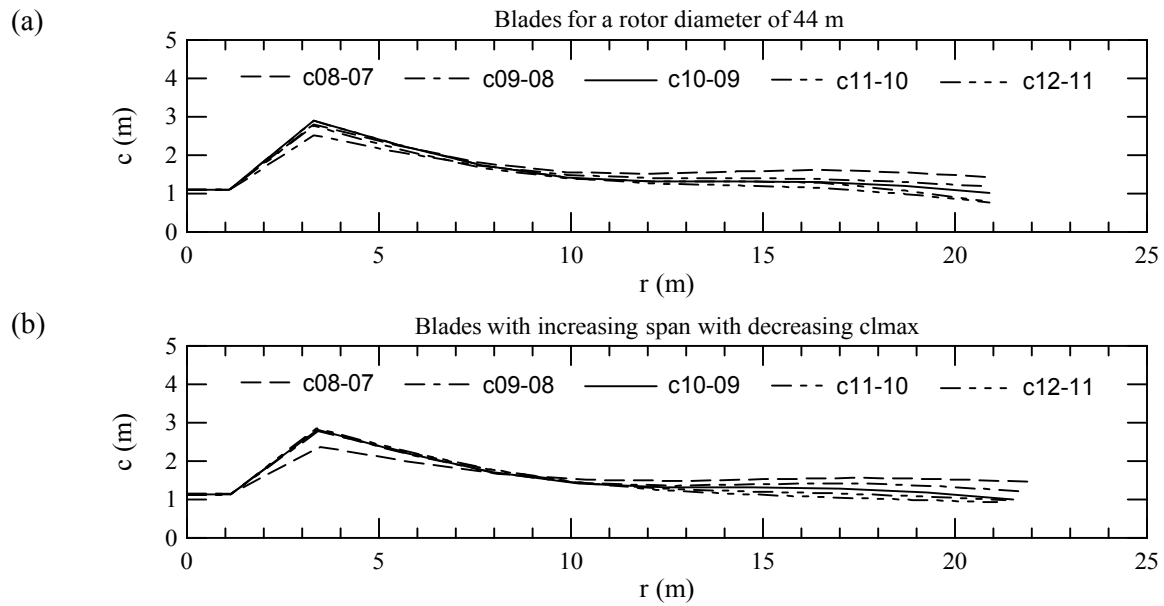


Fig. 6: Chord distributions for the cases considered in the optimization for maximum AEP: (a) fixed-rotor diameter and (b) increasing blade span with decreasing  $c_{l,max}$ .

### 3.2 Optimization for minimum COE

The COE results for the blades optimized for minimum COE are presented in Fig. 7. These results show again that the higher  $c_{l,max}$  cases provided the lowest COE for the two wind classes considered. As expected, the COE was largest in the case of the low wind regime (IEC wind class IV). The chord distributions are depicted in Fig. 8. The blades designed for IEC wind class II are almost identical. Consequently, the parked rotor in a 50-year extreme wind condition clearly drove the blade design, which explains the rather large inboard chords given the fixed airfoil thickness distribution. These inboard chords could be reduced to more practical values using a thicker root airfoil at the cost of increased roughness losses.<sup>20</sup> The ultimate load condition was less severe for the IEC wind class IV, and thus the differences in chord distributions were larger in that case. PROPGA found that slightly larger rotor diameters than the baseline (44.8–45.2 m) were optimum for IEC wind class IV, whereas the optimum rotor diameters for IEC wind class II were found to be essentially the same as the baseline value. Therefore, the rotor diameter seems to be more related to the wind regime than  $c_{l,max}$ .

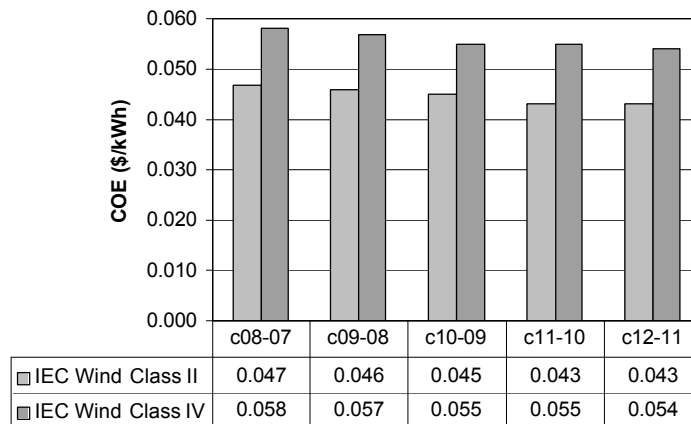


Fig. 7: Cost of energy for the cases considered in the optimization for minimum COE.

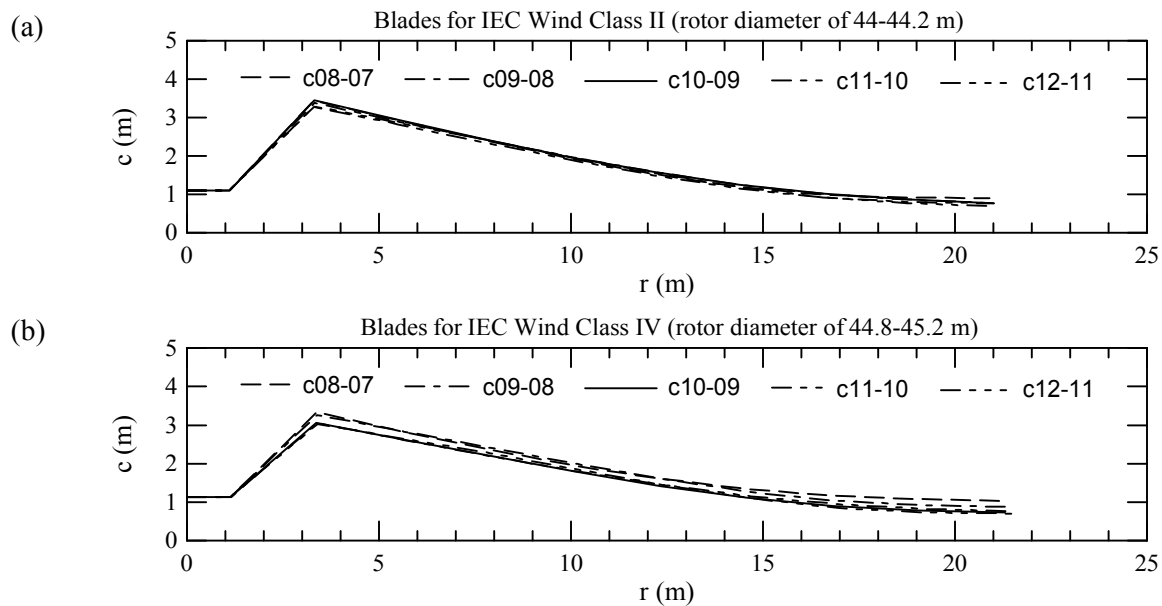


Fig. 8: Chord distributions for the cases considered in the optimization for minimum COE: (a) IEC wind class II and (b) IEC wind class IV.

### 3.3 Additional remarks

Although added complexity could have been included in the COE model, such as linking thrust and torque loads to tower and drive-train cost, respectively, the results shown in subsections 3.1 and 3.2 indicate that this was not necessary. Similar to the ultimate flap-bending loads considered in this study, the thrust loads scaled with blade area (fixed rated power). Therefore, linking the thrust loads to the tower cost would have increased the overall turbine cost when using airfoils having  $c_{l,max}$  in the lower end of the range considered as compared with using airfoils with  $c_{l,max}$  in the upper range. Also, because of the fixed rated power, the torque loads were basically identical. Consequently, adding complexity to the cost model would have increased the difference in the COE values between the design cases, but those results would have still favored the highest  $c_{l,max}$  cases over the lower ones. Finally, the total installed cost of the turbines was between \$750 and \$1100 per kW.

To limit the length of this paper, the optimized twist distributions and pitch settings were not presented because they were not needed to explain the trends in the results. Based on the nature of the synthesized airfoil data described in subsection 2.5, the optimized twist distributions and pitch settings were quite similar for all cases. The twist distributions were smooth and the blade pitch defined at 75% radius was between 2 and 3 degrees.

## 4. Conclusions

The results of this study on the blade design trade-offs using low-lift airfoils for stall-regulated HAWTs have led to the following conclusions and recommendations.

- For minimum COE, the ultimate flap-bending loads for the hurricane condition drive the design away from increasing the swept area with a reduction in  $c_{l,max}$ . Therefore, the swept area does not appear to be related to the  $c_{l,max}$  of the airfoils used.
- A  $c_{l,max}$  of 1.0 appears to be the lower practical limit for airfoils for stall-regulated HAWTs, unless there are other benefits to choosing lower  $c_{l,max}$ , such as for noise considerations.
- Higher  $c_{l,max}$  tip-region airfoils become more desirable as machine size increases.
- Future airfoil designs should seek to increase  $c_{l,max}$  while preserving gentle-stall characteristics.

These conclusions are likely to change, however, for other materials, such as carbon, and for smaller turbines because of Reynolds number effects and more importantly manufacturing issues, i.e., increasing  $c_{l,max}$  could lead to a chord length that is difficult, if not impossible to manufacture.

Gentle-stall characteristics have been desirable for stall-regulated HAWTs and should be beneficial for any wind turbines independent of the strategy used to control peak power. For pitch-regulated turbines that pitch towards feather, however, the need for gentle stall depends on the ability of the controller to keep the blades out of stall in gusty wind conditions.

## Acknowledgments

This work was undertaken with the support of the National Renewable Energy Laboratory under Subcontract No. XAF-5-14076-03 (technical monitor: J.L. Tangler). The authors would like to thank the following NREL employees for their helpful suggestions during the course of this work: Kirk Pierce, Walt Musial, Gunjit Bir, Marshall Buhl, and Brian Parsons.

## References

- <sup>1</sup> Tangler, J.L. and Somers, D.M., “Advanced Airfoils for HAWTs,” American Wind Energy Association WindPower '85 Conference, San Francisco, CA, August 17–20, 1985.
- <sup>2</sup> Tangler, J.L. and Somers, D.M., “Status of the Special-Purpose Airfoil Families,” American Wind Energy Association WindPower '87 Conference, San Francisco, CA, October 5–8, 1987.
- <sup>3</sup> Tangler, J.L., and Somers, D.M., “NREL Airfoil Families for HAWTs,” American Wind Energy Association WindPower '95 Conference, Washington, DC, March 26–30, 1995.
- <sup>4</sup> Tangler, J.L., Smith, B., and Jager, D., “SERI Advanced Wind Turbine Blades,” NREL/TP-257-4492, National Renewable Energy Laboratory (formerly the Solar Energy Research Institute), Golden, CO, February 1992.
- <sup>5</sup> Tangler, J.L., Kelley, N., Jager, D., and Smith, B., “Measured Structural Loads for the Micon 65/13,” NREL/TP-442-6062, National Renewable Energy Laboratory, Golden, CO, May 1994.
- <sup>6</sup> Huyer, S.A., Simms, D., and Robinson, M.C., “Unsteady Aerodynamics Associated with a Horizontal-Axis Wind Turbine,” *AIAA Journal*, Vol. 34, No. 7, July 1996, pp. 1410–1419.
- <sup>7</sup> Petersen, J.T., Madsen, H.A., Björck, A., Enevoldsen, P., Øye, S., Ganander, H., and Winkelaar, D., “Prediction of Dynamic Loads and Induced Vibrations in Stall,” Risø-R-1045(EN), Risø National Laboratory, Roskilde, Denmark, May 1998.
- <sup>8</sup> Selig, M.S. and Coverstone-Carroll, V.L., “Application of a Genetic Algorithm to Wind Turbine Design,” *ASME Journal of Solar Energy Engineering*, Vol. 118, March 1996, pp. 22–28.
- <sup>9</sup> Giguère, P. and Selig, M.S., “Aerodynamic Blade Design Methods for Horizontal Axis Wind Turbines,” 13<sup>th</sup> Annual Canadian Wind Energy Association Conference and Exhibition, Quebec City, Quebec, Canada, October 19–22, 1997.
- <sup>10</sup> Selig, M.S. and Tangler, J.L., “Development and Application of a Multipoint Inverse Design Method for Horizontal Axis Wind Turbines,” *Wind Engineering*, Vol. 19, No. 2, 1995, pp. 91–105.
- <sup>11</sup> Wilson, R.E. and Walker, S.N., “A FORTRAN Program for the Determination of Performance, Load and Stability Derivatives of Windmills,” Department of Mechanical Engineering, Oregon State University, Corvallis, Oregon, October, 1974.
- <sup>12</sup> Hibbs, B. and Radkey, R.L., “Calculating Rotor Performance with the Revised ‘PROP’ Computer Code,” *Horizontal-Axis Wind System Rotor Performance Model Comparison—A Compendium*, Wind Energy Research Center, Rockwell International, Rocky Flats Plant, Golden, CO, RFP-3508, UC-60, 1983.
- <sup>13</sup> Tangler, J.L. and Selig, M.S., “An Evaluation of an Empirical Model for Stall Delay Due to Rotation for HAWT,” American Wind Energy Association WindPower '97 Conference, Austin, TX, June 15–18, 1997.
- <sup>14</sup> Fuglsang, P.L. and Madsen, H.A., “A Design Study of a 1 MW Stall-regulated Rotor,” Risø-R-799(EN), Risø National Laboratory, Roskilde, Denmark, May 1995.

- <sup>15</sup> International Electrotechnical Commission, “IEC 61400-1, Ed. 2: Wind Turbine Generator Systems – Part 1: Safety Requirements”, FDIS 1998-12-15.
- <sup>16</sup> Sutherland, H., Beattie, A., Hansche, B., Musial, Walt, Allread, J., Johnson, J, and Summers, M., “The Application of Non-Destructive Techniques to the Testing of a Wind Turbine Blade,” SAND93-1380, Sandia National Laboratories, Albuquerque, New Mexico, June 1994.
- <sup>17</sup> Eppler, R. and Somers, D.M., “A Computer Program for the Design and Analysis of Low-Speed Airfoils, Including Transition,” NASA TM 80210, August 1980.
- <sup>18</sup> Somers, D.M., “Design and Experimental Results for the S809 Airfoil,” NREL/SR-440-6918, National Renewable Energy Laboratory, Golden, CO, January 1997.
- <sup>19</sup> Somers, D.M., “Design and Experimental Results for the S814 Airfoil,” NREL/SR-440-6919, National Renewable Energy Laboratory, Golden, CO, January 1997.
- <sup>20</sup> Somers, D.M., “Effect of Airfoil Thickness and Maximum Lift Coefficient on Roughness Sensitivity,” Airfoils Inc., State College, PA, October 1998.